



Published in final edited form as:

J Med Chem. 2018 April 12; 61(7): 3209–3217. doi:10.1021/acs.jmedchem.8b00343.

Nanomolar-Potency 1,2,4-Triazoloquinoxaline Inhibitors of the Kidney Urea Transporter UT-A1

Sujin Lee^{†,iD}, Onur Cil^{†,‡}, Elena Diez-Cecilia[§], Marc O. Anderson^{†,§,iD}, and Alan S. Verkman^{*,†}

[†]Departments of Medicine and Physiology, University of California, San Francisco, California 94143-0521, United States

[‡]Department of Pediatrics, Division of Nephrology, University of California, San Francisco, California 94143-0521, United States

[§]Department of Chemistry and Biochemistry, San Francisco State University, San Francisco, California 94132-1722, United States

Abstract

Urea transporter A (UT-A) isoforms encoded by the *Slc14a2* gene are expressed in kidney tubule epithelial cells, where they facilitate urinary concentration. UT-A1 inhibition is predicted to produce a unique salt-sparing diuretic action in edema and hyponatremia. Here we report the discovery of 1,2,4-triazoloquinoxalines and the analysis of 37 synthesized analogues. The most potent compound, **8ay**, containing 1,2,4-triazolo[4,3-*a*]quinoxaline-substituted benzenesulfonamide linked by an aryl ether, rapidly and reversibly inhibited UT-A1 urea transport by a noncompetitive mechanism with $IC_{50} \approx 150$ nM; the IC_{50} was ~ 2 μ M for the related urea transporter UT-B encoded by the *Slc14a1* gene. Molecular modeling suggested a putative binding site on the UT-A1 cytoplasmic domain. In vitro metabolism showing quinoxaline ring oxidation prompted the synthesis of metabolically stable 7,8-difluoroquinoxaline analogue **8bl**, which when administered to rats produced marked diuresis and reduced urinary osmolality. **8bl** has substantially improved UT-A1 inhibition potency and metabolic stability compared with prior compounds.

***Corresponding Author.** Address: 1246 Health Sciences East Tower, University of California, San Francisco, CA 94143-0521, U.S.A. Phone: 415 476-8530. Fax: 415 665-3847. Alan.Verkman@ucsf.edu. Web: www.ucsf.edu/verklab.

ORCID

Sujin Lee: 0000-0003-3345-2073

Marc O. Anderson: 0000-0002-1233-3801

ASSOCIATED CONTENT

Supporting Information The Supporting Information is available free of charge on the ACS Publications website at DOI: 10.1021/acs.jmedchem.8b00343.

Structures of active UT-A1 inhibitors identified by high-throughput screening, experimental details of in vitro microsomal stability assay, and synthesis details and spectroscopic characterization of synthesized compounds (PDF)

Structure of UT-A1 docked with **8bl** (PDB)

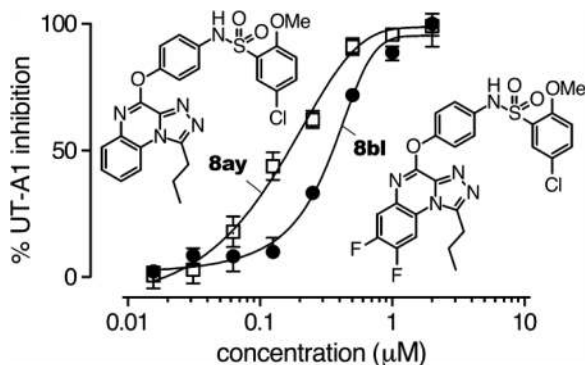
Molecular strings and IC_{50} data for all final inhibitor candidates (CSV)

Author Contributions

The manuscript was written through contributions of all authors. All authors have given approval to the final version of the manuscript.

The authors declare no competing financial interest.

Graphical abstract



INTRODUCTION

Urea transporters (UTs) in mammalian kidney are targets for the development of a new class of diuretics for the treatment of edema and hyponatremia in congestive heart failure, cirrhosis, nephrotic syndrome, and other disorders associated with fluid retention.^{1–6} Unlike available diuretics, UT inhibition disrupts the renal countercurrent mechanisms, which are required for the generation of a concentrated urine, producing a diuretic response with relative salt-sparing. Evidence for this mechanism comes from studies in transgenic mice lacking various UTs,^{7–13} from mathematical modeling of urinary concentration,¹⁴ and from rodent studies with administration of UT inhibitors.^{15–17}

Mammalian UTs are encoded by the genes *Slc14a2* (“UT-A” isoforms) and *Slc14a1* (“UT-B” isoform). UT-A isoforms are expressed in epithelial cells in kidney tubules, whereas UT-B is expressed in kidney vasa recta endothelia as well as in tissues outside of the kidney, including erythrocytes, testis, urinary bladder, heart, and brain.¹⁸ Of the various UT isoforms, the vasopressin-regulated UT-A1 in the inner medullary collecting duct is the principal target for UT-targeted diuretic development.¹⁹

The originally described UT inhibitors include millimolar-potency urea analogues^{20–22} and the nonselective membrane-intercalating agent phloretin.²³ Using an erythrocyte lysis assay, we originally identified highly selective UT-B inhibitors with IC₅₀ values down to 15 nM, which produced mild diuresis in mice.^{24,25} Subsequently, we developed a high-throughput screen to identify UT-A1 inhibitors using triply transfected MDCK cells expressing UT-A1, water channel aquaporin AQP1, and a yellow fluorescent protein (YFP) volume (chloride) sensor.²⁶ Screening produced UT-A1-selective inhibitors with low-micromolar potency and low to modest metabolic stability, which when delivered systemically in high doses to rats produced a diuretic response.²⁷ A recent study reported that UT-A and UT-B double-knockout mice showed increased urine output compared with the single-knockout mice,²⁸ suggesting the potential utility of nonselective UT inhibitors.

Here we report compounds with substantially improved UT-A1 inhibition potency and metabolic stability compared with prior compounds. Following high-throughput screening,

the 1,2,4-triazoloquinoxaline scaffold was selected for focused medicinal chemistry to optimize the UT-A1 inhibition potency and pharmacological properties.

RESULTS AND DISCUSSION

Screening and Scaffold Selection

Collections totaling ~150 000 drug-like synthetic small molecules were screened to identify inhibitors of rat UT-A1 using a cell-based fluorescence plate reader assay. Figures 1 and S1 show the structures of confirmed active compounds of at least 12 distinct chemical classes that produced >80% UT-A1 inhibition at 25 μ M. In order to select a scaffold for focused medicinal chemistry, we assayed 80 to 150 commercially available analogues of each class (**1–4**, **S1–S7**, and **8aa**) with the primary goal of high-potency UT-A1 inhibition and a secondary goal of some UT-B inhibition. A common characteristic of the UT-A1 inhibitors was a linear multiheterocyclic structure such as in **1** and **2**. However, these linear multiheterocyclic structures showed little UT-B inhibition, which was also the case for 2-phenylquinoline **3**. Compound **4** has a similar thienoquinoline structure as previously reported **PU-48**²⁹ and has low potency for UT-A1 inhibition. Another common structural motif of compounds with the greatest UT-A1 inhibition potency was a substituted benzenesulfonamide linked to an aromatic ring, such as in **5**,²⁶ **6**, **7**, and **8aa**. Of the benzenesulfonamide analogues, 1,2,4-triazolo[4,3-*a*]quinoxaline **8aa** had the greatest UT-A1 inhibition potency with $IC_{50} \approx 0.8 \mu$ M while retaining modest activity against UT-B. On the basis of consideration of the potencies against UT-A1 and UT-B, drug-like properties, modularity of construction, and presence of hydrogen-bond-donating and -accepting functionality, focused medicinal chemistry was done here on the 4-oxyphenyl-1,2,4-triazolo[4,3-*a*]quinoxaline scaffold (**8**). Compounds having the general 1,2,4-triazolo[4,3-*a*]quinoxaline scaffold, though quite distinct from those studied here, have been reported as adenosine receptor antagonists³⁰ and inhibitors of the folate cycle,³¹ BET,³² and PDE2.³³

Preliminary structure–activity studies of 156 commercial analogues of **8aa** indicated that a substituted benzenesulfonamide on the 4-oxyaniline group was important for UT-A1 inhibition (Figure S1). Analogues of **8aa** in which the sulfonamide was replaced with NH_2 , OH, or H were inactive. Compounds linked through an amide instead of sulfonamide were inactive, as were 2,4-disubstituted benzenesulfonamides or 2-thiophenesulfonamide. In general, the most active compounds contained a 4-oxyaniline moiety linked via a sulfonamide to a 2,5-disubstituted benzene.

Our exploration of the structure–activity relationship (SAR) of this scaffold focused on four distinct components (Figure 1B), including (A) modification of the X group (ether and amine linkages), (B) benzenesulfonamide substitutions, (C) alkyl incorporation on the 1,2,4-triazole moiety, and (D) disubstitution on the triazoloquinoxaline backbone.

Chemistry

Scheme 1 shows the synthetic route developed for 5-alkyl-1,2,4-triazoloquinoxaline analogues in four steps from commercially available 2,3-dichloroquinoxaline (**9**). Monosubstitution with hydrazine on 2,3-dichloroquinoxaline afforded

hydrazinylquinoxaline **10**, which was condensed with triethyl orthoformate to give triazoloquinoxaline **11a**. Nucleophilic aromatic substitution with 4- or 3-aminophenol in the presence of cesium carbonate in DMSO yielded **12a** and **12b**, respectively. Use of cesium carbonate ensured deprotonation of the phenol to enhance the nucleophilicity of the oxygen, preventing attack by nitrogen. Nucleophilic substitution with *p*- or *m*-phenylenediamine in the presence of potassium carbonate yielded N-substituted intermediates **12c** and **12d**, respectively. Subsequently, **12a–d** were reacted with various substituted benzenesulfonyl chlorides to give **8aa–am** (see Table 1). To vary substitution at the R² position, hydrazinylquinoxaline **10** was reacted with various trialkyl orthoalkanoates to generate **11b–g**. These intermediates were similarly reacted with *p*-aminophenol to yield aminobenzenes **12e–j**. Lastly, these intermediates were conjugated with a focused collection of substituted benzenesulfonyl chlorides to generate **8an–bd** (see Table 2).

Initial microsomal stability experiments on **8aa** as described below suggested the electron-rich 1,2,4-triazoloquinoxaline heteroaryl ring to be susceptible to oxidation. On this basis, and to explore the importance of part D, we devised a synthesis allowing variation of this region (Scheme 2). Several 6,7-disubstituted 2,3-dichloroquinoxalines (**13a–c**) were transformed to the hydrazine derivatives (**14a–c**), cyclized to the 1,2,4-triazoloquinoxalines (**15a–g**) using appropriate trialkyl orthoformate or orthoalkane species, and then coupled with *p*-aminophenol to obtain the aminobenzene derivatives (**16a–g**). Lastly, a focused selection of substituted benzenesulfonyl chlorides were coupled to generate **8be–bl** (see Table 3). We found some of the 1,2,4-triazoloquinoxalines (**15**) and 4-aminophenol-conjugated intermediates (**16**) difficult to purify. Fortunately, the sequence **15** → **16** → **8** could often be “tunneled” without purification of each synthetic intermediate but with the final products isolated in high purity. The selection of the *p*-aminophenol linkage as well as a small set of R¹ and R² groups in this series was based on SAR that emerged from the previous set of compounds in Tables 1 and 2.

Structure–Activity Analysis

UT-A1 inhibition data for all of the compounds (**8aa–bl**) are summarized in Tables 1–3. We first examined the substitution pattern of the aryl linker (part A) (Table 1). The *p*-aminophenol linker in **8aa** resulted in greater UT-A1 inhibition potency compared with similar compounds linked with *m*-aminophenol (**8ab**), *p*-diaminobenzene (**8ac** and **8am**), or *m*-diaminobenzene (**8ad**).

Variation of R¹ (the benzenesulfonamide, part B) showed that 2,5-disubstituted benzenes were favored, with 5-chloro-2-methoxy (**8aa**) having the greatest potency, while compounds containing 5-methyl-2-methoxy (**8ae**) and 2,5-dimethyl (**8af**) were less potent and the compound with 2-chloro-5-methoxy (**8ag**) was inactive. Compounds with a single ortho or meta substituent on the benzenesulfonamide (**8ah–ak**) were substantially less potent and not further explored.

The R² substituent was varied next (Table 2), maintaining the most promising 2,5-disubstituted benzenesulfonamides at R¹. Short, linear, and branched alkyl groups at R² were investigated because of their ease of installation, although ethoxy was also possible

using our synthetic scheme. Varying the length of alkyl group at R² showed that propyl (**8ay**) was best, while butyl (**8bb**) and isopropyl (**8at**) were comparable, ethyl (**8aq**) and ethoxy (**8aw**) were slightly worse, and methyl (**8an**) was inactive. Across this series (and the compounds listed in Table 1), the 5-chloro-2-methoxy group at R¹ appeared to be better than 5-methyl-2-methoxy and 2,5-dimethyl.

Lastly, variation of the R³ substituent was explored (Table 3). Methyl substitution (**8be–bh**) produced less potent inhibitors than the analogous unsubstituted derivatives (**8aa**, **8aq**, **8at**, **8ay**), although propyl at R² (**8bh**) achieved the best potency in the subset. Also, we observed that the relation of alkyl chain length and branching to inhibition potency was similar to that for the unsubstituted analogues. A dichloro-substituted compound (**8bi**) was inactive, while difluoro at R³ was tolerated in three analogues (**8bj–bl**). Among the R³-substituted compounds, **8bl** was the most potent, preserving the propyl substituent at R² (IC₅₀ = 0.3 μM), although it was less potent than the analogous unsubstituted compound **8ay** (IC₅₀ = 0.15 μM).

Functional Studies

Figure 2A shows original fluorescence plate reader data for inhibition of UT-A1 urea transport in MDCK cells. Curves are shown for zero inhibition (blue, DMSO vehicle control), 100% inhibition (red, phloretin), and different concentrations of **8ay**. The deduced concentration–inhibition curves for **8ay** as well as for **8aa** and **8bl** are shown in Figure 2B, and Figure 2C shows concentration–inhibition curves for rat UT-B, with IC₅₀ values of 2, 4, and 0.8 μM for **8ay**, **8aa** and **8bl**, respectively. For comparison, the previously reported thienoquinoline **PU-48**²⁹ showed weak and partial UT-A1 inhibition but better inhibition potency for UT-B.

The most potent analogue, **8ay**, was further characterized for reversibility, inhibition mechanism, and kinetics. Reversibility was studied by incubation of cells with 0.5 μM **8ay** for 15 min followed by washing and assay of UT-A1 inhibition. Inhibition was fully reversed (Figure 2D). The IC₅₀ values for **8ay** inhibition of UT-A1 urea transport measured using different urea concentration gradients (200, 400, and 800 mM) were similar (Figure 2E), suggesting a noncompetitive inhibition mechanism. Measurement of the kinetics of UT-A1 inhibition following **8ay** addition showed little immediate inhibition and a half-time for inhibition of ~2 min (Figure 2F), suggesting an intracellular site of action. Cytotoxicity was not observed at a high concentration (10 μM) for several compounds tested (Figure 2G).

Molecular Docking

Figure 3 shows a docked conformation of **8bl** bound to a previously described homology model of the UT-A1 cytoplasmic domain.²⁶ In the docked conformation, the central triazoloquinoxaline heterocycle is positioned near several hydrophobic residues around the entrance of the cytoplasmic channel, including Leu652, Pro705, Leu895, and Val898. The hydrophobic propyl (R² substituent) projects deeper into the cavity, surrounded by the side chains of Gln599, Phe602, Tyr655, and Phe832. The 4-oxyaniline linker group extends outward from the channel, near Ser696 and Val706, while the substituted

benzenesulfonamide resides completely outside the channel, making contacts with the cytoplasmic surface of the protein (nearest to Asp644, Leu895, and Ser896). Notably, a broader series of active analogues of **8bl** were also docked (data not shown), giving a similar binding orientation of the triazoloquinoxaline with alkyl substituents at R² projecting into the channel. For comparison, in the docked pose of the inactive analogue **8am** (Figure S3), the triazoloquinoxaline and substituted benzenesulfonamide ring systems are flipped into an opposite orientation, and this compound lacks a hydrophobic substituent extending into the channel.

In Vitro Metabolic Stability

In vitro metabolic stability was measured by compound incubation with rat hepatic microsomes at 37 °C for different times in the presence of NADPH, followed by LC/MS analysis. Figure 4A shows the time course of metabolism for the relatively potent quinoxalines **8ay**, **8bh**, and **8bl** (each containing propyl at R²). Compounds **8ay** (R³ = H) and **8bh** (R³ = CH₃) were rapidly degraded at 15 min, with 40% and 25% remaining, respectively, in contrast to **8bl** (R³ = F), which was substantially more stable, with 60% remaining at 30 min. Degradation of **8ay** (*m/z* 524) was paralleled with an increase in the signal at *m/z* 540 (Figure 4B), consistent with hydroxylation, suggesting that the fluoro substituent in **8bl** (R³ = F) prevented hydroxylation at this position (Figure 4C), explaining its relative stability compared with **8ay**. The rapid metabolism of **8bh** was not explored but could be due to hydroxylation of the two benzylic methyl groups. In vivo studies in rats were done using the relatively stable and potent **8bl**.

Rat Pharmacokinetics and Efficacy

After preliminary testing of different administration routes (oral, intraperitoneal, intravenous), intravenous administration of **8bl** at 4 mg/kg yielded serum concentrations greater than 2 μM for 3 h (Figure 5A, left) and urine concentrations of 6–8 μM for 3 h (Figure 5A, right), each well above the IC₅₀ of 0.3 μM for UT-A1 inhibition by **8bl** determined in vitro. Intravenous administration of **8bl** at 4 mg/kg significantly increased the 3 h urine volume and reduced the urine osmolality compared with pretreatment values (Figure 5B,C), whereas administration of vehicle did not significantly change the 3 h urine volume or osmolality.

CONCLUSION

The 1,2,4-triazolo[4,3-*a*]quinoxaline analogues identified and characterized here are substantially more potent and metabolically stable than previously described UT-A1 inhibitors. Inhibition of UT-A1-mediated urea transport was rapid, reversible, and noncompetitive and probably involves inhibitor binding at the cytoplasmic surface of UT-A1 near but distinct from the urea binding site. Following structure–activity analysis, which resulted in improved metabolic stability by difluoro substitution on the triazoloquinoxaline backbone, **8bl** was found to have favorable pharmacokinetics in rats and produced a diuretic response. These results support further preclinical development of 1,2,4-triazolo[4,3-*a*]quinoxalines as first-in-class diuretics targeting kidney urea transporters.

EXPERIMENTAL SECTION

General

All of the solvents and chemicals were used as purchased without further purification. Reagents were purchased from Sigma-Aldrich (St. Louis, MO), Alfa Aesar (Haverhill, MA), TCI America (Portland, OR), and Maybridge. Reaction progress was monitored on Merck precoated silica gel plates (with fluorescence at 254 nm) using ethyl acetate/*n*-hexane as the solvent system. Column chromatography was done with Fluka silica gel 60 (230–400 mesh). Proton (¹H) and carbon (¹³C) NMR spectra were recorded on a Bruker Avance 300 (300 MHz for ¹H; 75 MHz for ¹³C) or 500 (500.13 MHz for ¹H; 125.76 MHz for ¹³C) spectrometer using CDCl₃, CD₃OD, or DMSO-*d*₆ as solvents. Chemical shifts are given in parts per million (ppm). High-resolution mass spectrometry (HRMS) was performed using a hybrid quadrupole Orbitrap mass analyzer, QExactive (Thermo, Bremen, Germany), with an electrospray ionization source. The mass resolution was set as 70 000 at *m/z* 200, and the mass accuracy was better than 3 ppm. The purity of all final compounds was 95% or higher, as determined by high-performance liquid chromatography (HPLC) using UV absorbance at 254 nm. HPLC was done on an Xterra MS C18 column (2.1 mm × 100 mm, 3.5 μm) with 0.2 mL/min water/acetonitrile (containing 0.1% formic acid), 24 min linear gradient, 5–95% acetonitrile.

Syntheses

N-(4-([1,2,4]Triazolo[4,3-a]quinoxalin-4-yloxy)-phenyl)-5-chloro-2-methoxybenzenesulfonamide (8aa)—To a suspension of 4-oxyphenylquinoxaline amine **12a** (70 mg, 0.25 mmol) in acetonitrile (7 mL) was added DIPEA (0.07 mL, 0.5 mmol) and 2-methoxy-5-chlorobenzenesulfonyl chloride (61 mg, 0.25 mmol). The mixture was stirred overnight at 60 °C. After the reaction mixture was cooled to room temperature, water (7 mL) was added, resulting in the formation of the product as a precipitate, which was dried in vacuo to afford the product as a yellow solid (70 mg, 58%). ¹H NMR (300 MHz, DMSO-*d*₆) δ 10.28 (brs, 1H), 10.16 (s, 1H), 8.37 (d, 1H, *J* = 8.0 Hz), 7.74 (d, 1H, *J* = 2.7 Hz), 7.70 (d, 1H, *J* = 2.7 Hz), 7.68–7.56 (m, 3H), 7.31 (d, 2H, *J* = 9.0 Hz), 7.31–7.26 (m, 1H), 7.21 (d, 2H, *J* = 9.0 Hz), 3.91 (s, 3H); ¹³C NMR (75 MHz, DMSO-*d*₆) δ 155.8, 151.4, 148.6, 138.7, 138.6, 135.6, 135.1, 134.1, 129.6, 128.5, 128.2, 128.1, 127.8, 124.5, 124.1, 123.0, 121.9, 116.9, 115.5, 57.0; HRMS *m/z* (ESI) calcd for C₂₂H₁₆ClN₅O₄S [M + H]⁺ 482.0673, found 482.0685.

2-Chloro-3-hydrazinylquinoxaline (10)—A solution of 2,3-dichloroquinoxaline (**9**) (14.0 g, 69.6 mmol) and hydrazine monohydrate (3.5 mL, 70.0 mmol) in ethanol (250 mL) was stirred overnight at ambient temperature. The resulting precipitate was filtered using a Büchner funnel under reduced pressure, washed with ice-cold ethanol (20 mL), and dried in vacuo to give **10** as a yellow powder (13.3 g, 97.8%). ¹H NMR (300 MHz, CDCl₃) δ 7.88 (dd, 1H, *J* = 1.2, 8.1 Hz), 7.85 (dd, 1H, *J* = 1.2, 8.4 Hz), 7.65 (ddd, 1H, *J* = 1.2, 1.5, 8.4 Hz), 7.48 (ddd, 1H, *J* = 1.5, 8.1, 8.4 Hz), 4.18 (brs, 1H).

4-Chloro-[1,2,4]triazolo[4,3-a]quinoxaline (11a)—A mixture of hydrazinylquinoxaline **10** (6.0 g, 30.8 mmol) and triethyl orthoformate (50 mL, 300 mmol)

was stirred at 100 °C for 1 h. After cooling, the reaction mixture was filtered using a Büchner funnel under reduced pressure, washed with cyclohexane (10 mL), and dried in vacuo to give **11a** as a yellow solid (4.0 g, 63%). ¹H NMR (300 MHz, DMSO-*d*₆) δ 10.2 (s, 1H), 8.46 (dd, 1H, *J* = 0.9, 8.2 Hz), 8.04 (dd, 1H, *J* = 0.9, 8.1 Hz), 7.88–7.70 (m, 2H); ¹³C NMR (75 MHz, DMSO-*d*₆) δ 139.3, 138.9, 134.8, 130.7, 129.4, 128.6, 128.4, 125.3, 117.2; LRMS (ESI) *m/z* 205 [M + H]⁺.

4-([1,2,4]Triazolo[4,3-a]quinoxalin-4-yloxy)aniline (12a)—To a solution of quinoxaline **11a** (300 mg, 1.5 mmol) in DMSO (4 mL) were added 4-aminophenol (160 mg, 1.5 mmol) and cesium carbonate (580 mg, 1.8 mmol). The mixture was heated to 80 °C for 1.5 h. After cooling to room temperature, the reaction mixture was diluted with CH₂Cl₂ (10 mL) and acidified with 1 N HCl, and the resulting precipitate was filtered using a Büchner funnel under reduced pressure to give **12a** as an olive-green solid (300 mg, 74%). ¹H NMR (300 MHz, DMSO-*d*₆) δ 10.20 (d, 1H, *J* = 5.4 Hz), 8.36 (d, 1H, *J* = 7.9 Hz), 7.68–7.55 (m, 3H), 7.05 (d, 2H, *J* = 8.7 Hz), 6.67 (d, 2H, *J* = 8.7 Hz), 5.14 (s, 2H); ¹³C NMR (75 MHz, DMSO-*d*₆) δ 152.1, 147.1, 142.2, 138.79, 138.70, 134.5, 128.2, 128.1, 127.5, 124.4, 122.5, 116.8, 114.7; LRMS (ESI) *m/z* 278 [M + H]⁺.

Cell Culture

As described previously,³⁴ MDCK cells stably expressing rat UT-A1, YFP-H148Q/V163S, and human AQP1 were grown in Dulbecco's modified Eagle's medium (DMEM) containing 10% fetal bovine serum (FBS), penicillin G (100 units/mL), streptomycin (100 µg/mL), zeocin (500 µg/mL), Geneticin (750 µg/mL), and hygromycin (500 µg/mL) at 37 °C, 5% CO₂. A cell clone with bright YFP fluorescence and relatively low AQP1 expression was used to maximize the dynamic range.

In Vitro Functional Studies

Reversibility of UT-A1 inhibition was tested by preincubating the UT-A1-expressing MDCK cells with **8ay** (0.5 µM) for 10 min and then washing the cells with PBS prior to assay. The kinetics of UT-A1 inhibition was measured by adding **8ay** (0.5 µM) at different times prior to the assay. The urea concentration dependence of UT-A1 inhibition was studied from inhibitor concentration–response data using different urea gradients.

UT-B Inhibition Measurements

As described previously,³⁴ whole rat blood was diluted to a hematocrit of ~1.5% in PBS containing 1.25 M acetamide and 5 mM glucose. Erythrocyte suspensions (100 µL) were added to 96-well round-bottom microplates, and test compounds (1 µL) were added. After 15 min of incubation, 20 µL of the erythrocyte suspension was added rapidly to each well. Following vigorous mixing, erythrocyte lysis was quantified by absorbance (Abs) at 710 nm. A nonlysed control (isomolar buffer) and a lysed control (0.7 mM phloretin) were added to each plate as negative and positive controls, respectively. Percentage erythrocyte lysis was calculated as % lysis = 100% × (Abs_{neg} – Abs_{test})/(Abs_{neg} – Abs_{pos}).

Cell Toxicity

Transfected MDCK cells on black 96-well Costar microplates with clear plastic bottoms were cultured for 24 h at 37 °C and incubated with test compounds (10 µM) for 24 h. Cell viability was assayed using AlamarBlue (Pierce, Rockford, IL).

Homology Modeling and Docking Computations

A homology model of rat UT-A1 had been previously generated.²⁶ The homology models were prepared for docking using the FRED-RECEPTOR utility (version 2.2.5; OpenEye Scientific Software, Santa Fe, NM; <http://www.eyesopen.com>), with cytoplasmic and extracellular domains defined with 10 cubic Å boxes. Structures of the relevant inhibitor molecules were converted to SMILES strings, transformed to three-dimensional conformations, and minimized using PIPELINE PILOT (Accelrys, San Diego, CA). Single conformations were passed through MOLCHARGE (version 1.5.0; OpenEye Scientific Software) to apply MMFF charges and through OMEGA (version 2.4.6; OpenEye Scientific Software) to generate multi-conformational libraries, which were docked using FRED (version 2.2.5; OpenEye Scientific Software) with the consensus scoring functions ChemGauss3, ChemScore, OEChemScore, ScreenScore, ShapeGauss, PLP, and ZapBind. Bound complexes were visualized using PyMOL (Schrödinger, LLC, San Diego, CA).

In Vitro Metabolic Stability

Compounds (5 µM) were preincubated for 5 min at 37 °C with rat liver microsomes (Sprague-Dawley, male; 1 mg of protein/mL; Sigma-Aldrich, St. Louis, MO) in PBS (0.1 M, pH 7.4), and then 1 mM NADPH was added, after which the mixtures were incubated for specified times at 37 °C. The mixtures were then chilled on ice, and 0.5 mL of ice-cold EtOAc was added. Samples were centrifuged for 15 min at 3000 rpm, and the supernatant was evaporated to dryness. Then the residues were dissolved in 100 µL of mobile phase (3:1 acetonitrile/water containing 0.1% formic acid) for LC/MS. Reversed-phase HPLC separations were carried out using an Xterra MS C18 column (2.1 mm × 100 mm, 3.5 µm) equipped with a solvent delivery system (model 2695, Waters, Milford, MA) using a linear gradient from 5 to 95% acetonitrile containing 0.1% formic acid, run over 24 min at a flow rate of 0.2 mL/min. The peak area/internal area ratio was plotted over incubation time. MassLynx 4.1 was used to analyze the data.

Rat Pharmacokinetics

Procedures herein were approved by the Committee on Animal Research at the University of California, San Francisco. Rats (Wistar males, 250–300 g) were purchased from Charles River Laboratories (Wilmington, MA). Rats were acclimated by placing them individually in metabolic cages for 3 consecutive days (6 h per day) before the experiments. Compound **8bl** was administered intravenously using a 24-gauge catheter at 4 mg/kg in saline containing 20% dimethylacetamide and 1.28 mg/mL NaOH in saline (total administered volume of ~1 mL per rat). Blood samples (250 µL) were collected via tail vein puncture at 15, 30, 60, 120, and 180 min in plain tubes with no anticoagulant, and serum was separated by centrifugation at 5000 rpm for 15 min. Urine was collected in metabolic cages for 3 h after injection at room temperature. Serum and urine samples were kept frozen at –20 °C until analysis.

Calibration standards were prepared in urine and plasma from control (non-treated) rats to which known amounts of pure **8bl** were added. The mixtures were centrifuged for 20 min at 13 200 rpm, and 90 μ L aliquots of supernatants were taken for LC/MS. LC/MS analysis was performed with a Waters 2695 separation module coupled to a Waters Micromass ZQ mass spectrometer using ESI-positive ionization and masses ranging from 100 to 1500 Da (40 V cone voltage).

Diuretic Studies in Rats

Compound **8bl** was administered to rats as described above for pharmacokinetics studies. Rats were placed in metabolic cages individually with water and food available ad libitum before and during experiments. Spontaneously voided urine was collected for 3 h, and then compound or vehicle treatment was given intravenously. Urine was collected for 3 h after treatments. The urine volume was quantified, and the urine osmolality was measured using freezing point depression osmometry (Precision Systems).

Supplementary Material

Refer to Web version on PubMed Central for supplementary material.

Acknowledgments

This work was supported by National Institutes of Health Grants DK101373, DK72517, DK099803, and EY13574. The authors thank Dr. Robert Yen of the SFSU Mass Spectrometry Facility for HRMS measurements, funded by National Science Foundation Grant CHE-1228656.

ABBREVIATIONS USED

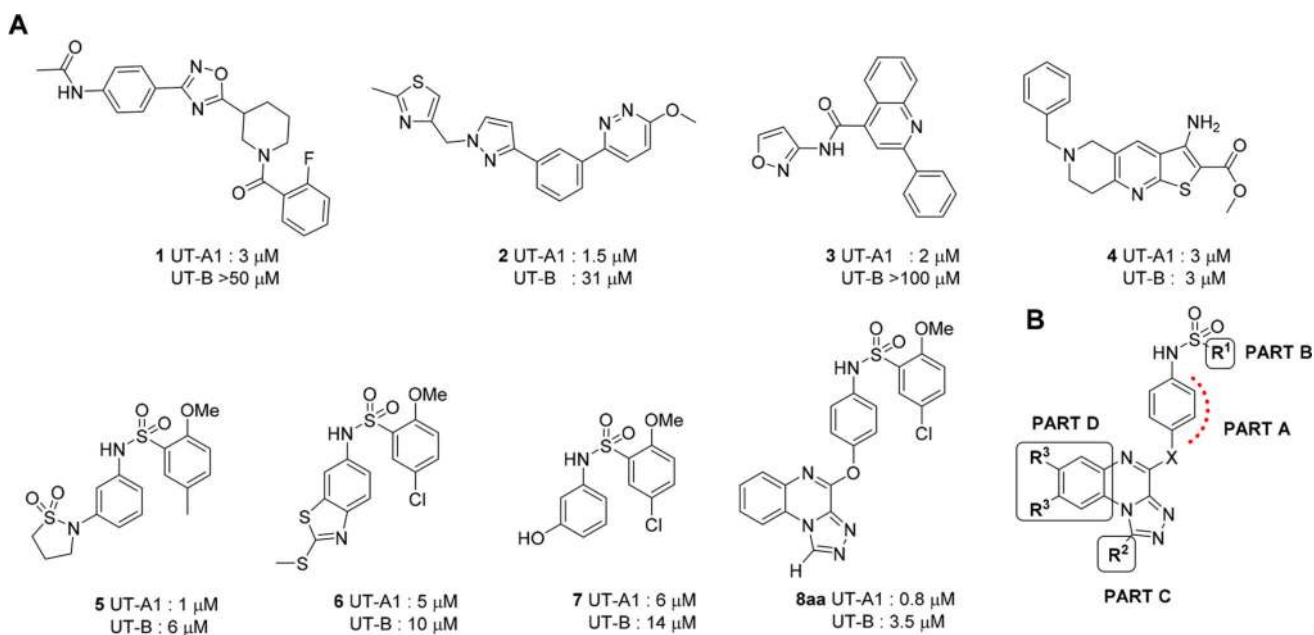
UT	Urea Transporter
DIPEA	<i>N,N</i> -diisopropyl ethylamine
DMSO	dimethyl sulfoxide
SAR	structure–activity relationship
MDCK	Madin-Darby canine kidney
AQP1	Aquaporin-1
PBS	phosphate buffered saline
SEM	standard error of the mean

References

1. Klein JD, Sands JM. Urea transport and clinical potential of urearetics. *Curr. Opin. Nephrol. Hypertens.* 2016; 25:444–451. [PubMed: 27367911]
2. Smith CP. Mammalian urea transporters. *Exp. Physiol.* 2009; 94:180–185. [PubMed: 19028811]
3. Klein JD, Blount MA, Sands JM. Urea transport in the kidney. *Compr. Physiol.* 2011; 1:699–729. [PubMed: 23737200]

4. Yang, B., Sands, JM., editors. Subcellular Biochemistry. Vol. 73. Springer; New York: 2014. Urea Transporters.
5. Yang B, Bankir L. Urea and urine concentrating ability: new insights from studies in mice. *Am. J. Physiol. Renal Physiol.* 2005; 288:F881–F896. [PubMed: 15821253]
6. Klein JD, Blount MA, Sands JM. Molecular mechanisms of urea transport in health and disease. *Pfluegers Arch.* 2012; 464:561–572. [PubMed: 23007461]
7. Yang B, Bankir L, Gillespie A, Epstein CJ, Verkman AS. Urea selective concentrating defect in transgenic mice lacking urea transporter UT-B. *J. Biol. Chem.* 2002; 277:10633–10637. [PubMed: 11792714]
8. Bankir L, Chen K, Yang B. Lack of UT-B in vasa recta and red blood cells prevents urea-induced improvement of urinary concentrating ability. *Am. J. Physiol. Renal Physiol.* 2004; 286:F144–151. [PubMed: 12965892]
9. Fenton RA, Chou CL, Stewart GS, Smith CP, Knepper MA. Urinary concentrating defect in mice with selective deletion of phloretin sensitive urea transporters in the renal collecting duct. *Proc. Natl. Acad. Sci. U. S. A.* 2004; 101:7469–7474. [PubMed: 15123796]
10. Fenton RA, Flynn A, Shodeinde A, Smith CP, Schnermann J, Knepper MA. Renal phenotype of UT-A urea transporter knockout mice. *J. Am. Soc. Nephrol.* 2005; 16:1583–1592. [PubMed: 15829709]
11. Uchida S, Sohara E, Rai T, Ikawa M, Okabe M, Sasaki S. Impaired urea accumulation in the inner medulla of mice lacking the urea transporter UT-A2. *Mol. Cell. Biol.* 2005; 25:7357–7363. [PubMed: 16055743]
12. Klein JD, Frohlich O, Mistry AC, Kent KJ, Martin CF, Sands JM. Transgenic mice expressing UT-A1, but lacking UT-A3, have intact urine concentration ability. *FASEB J.* 2013; 27(Suppl. 1): 1111–17.
13. Klein JD, Wang Y, Mistry A, LaRocque LM, Molina PA, Rogers RT, Blount MA, Sands JM. Transgenic restoration of urea transporter A1 confers maximal urinary concentration in the absence of urea transporter A3. *J. Am. Soc. Nephrol.* 2016; 27:1448–1455. [PubMed: 26407594]
14. Layton AT. A mathematical model of the urine concentrating mechanism in the rat renal medulla. I. Formulation and base-case results. *Am. J. Physiol. Ren. Physiol.* 2011; 300:F356–F371.
15. Cil O, Ertunc M, Onur R. The diuretic effect of urea analog dimethylthiourea in female Wistar rats. *Hum. Exp. Toxicol.* 2012; 31:1050–1055. [PubMed: 23023029]
16. Li F, Lei T, Zhu J, Wang W, Sun Y, Chen J, Dong Z, Zhou H, Yang B. A novel small-molecule thienoquinolin urea transporter inhibitor acts as a potential diuretic. *Kidney Int.* 2013; 83:1076–1086. [PubMed: 23486518]
17. Cil O, Esteva-Font C, Tas ST, Su T, Lee S, Anderson MO, Ertunc M, Verkman AS. Salt-sparing diuretic action of a water-soluble urea analog inhibitor of urea transporters UT-A and UT-B in rats. *Kidney Int.* 2015; 88:311–320. [PubMed: 25993324]
18. Esteva-Font C, Anderson MO, Verkman AS. Urea transporter proteins as targets for small-molecule diuretics. *Nat. Rev. Nephrol.* 2015; 11:113–123. and references therein. [PubMed: 25488859]
19. Sands JM. Urea transporter inhibitors: en route to new diuretics. *Chem. Biol.* 2013; 20:1201–1202. [PubMed: 24210002]
20. Mayrand RR, Levitt DG. Urea and ethylene glycol-facilitated transport systems in the human red cell membrane. Saturation, competition, and asymmetry. *J. Gen. Physiol.* 1983; 81:221–237. [PubMed: 6842173]
21. Martial S, Neau P, Degeilh F, Lamotte H, Rousseau B, Ripoche P. Urea derivatives as tools for studying the urea-facilitated transport system. *Pfluegers Arch.* 1993; 423:51–58. [PubMed: 8488092]
22. Esteva-Font C, Phuan PW, Lee S, Su T, Anderson MO, Verkman AS. Structure-activity analysis of thiourea analogs as inhibitors of UT-A and UT-B urea transporters. *Biochim. Biophys. Acta, Biomembr.* 2015; 1848:1075–1080.
23. Chou CL, Knepper MA. Inhibition of urea transport in inner medullary collecting duct by phloretin and urea analogues. *Am. J. Physiol. Renal Physiol.* 1989; 257:F359–365.

24. Anderson MO, Zhang J, Liu Y, Yao C, Phuan PW, Verkman AS. Nanomolar potency and metabolically stable inhibitors of kidney urea transporter UT-B. *J. Med. Chem.* 2012; 55:5942–5950. [PubMed: 22694147]
25. Yao C, Anderson MO, Zhang J, Yang B, Phuan PW, Verkman AS. Triazolothienopyrimidine inhibitors of urea transporter UT-B reduce urine concentration. *J. Am. Soc. Nephrol.* 2012; 23:1210–1220. [PubMed: 22491419]
26. Esteva-Font C, Phuan PW, Anderson MO, Verkman AS. A small molecule screen identifies selective inhibitors of urea transporter UT-A. *Chem. Biol.* 2013; 20:1235–1244. [PubMed: 24055006]
27. Esteva-Font C, Cil O, Phuan PW, Su T, Lee S, Anderson MO, Verkman AS. Diuresis and reduced urinary osmolality in rats produced by small-molecule UT-A-selective urea transport inhibitors. *FASEB J.* 2014; 28:3878–3890. [PubMed: 24843071]
28. Jiang T, Li J, Layton AT, Wang W, Sun W, Li M, Zhou H, Yang B. Generation and phenotypic analysis of mice lacking all urea transporters. *Kidney Int.* 2017; 91:338–351. [PubMed: 27914708]
29. Ren H, Wang Y, Xing Y, Ran J, Liu M, Lei T, Zhou H, Li R, Sands JM, Yang B. Thienoquinolins exert diuresis by strongly inhibiting UT-A urea transporters. *Am. J. Physiol. Renal Physiol.* 2014; 307:F1363–F1372. [PubMed: 25298523]
30. (a) Catarzi D, Colotta V, Varano F, Lenzi O, Filacchioni G, Trincavelli L, Martini C, Montopoli C, Moro S. 1,2,4-Triazolo[1,5-*a*]quinoxaline as a versatile tool for the design of selective human A3 adenosine receptor antagonists: synthesis, biological evaluation, and molecular modeling studies of 2-(hetero)aryl- and 2-carboxy-substituted derivatives. *J. Med. Chem.* 2005; 48:7932–7945. [PubMed: 16335918] (b) Vernall AJ, Stoddart LA, Briddon SJ, Hill SJ, Kellam B. Highly potent and selective fluorescent antagonists of the human adenosine A3 receptor based on the 1,2,4-Triazolo[4,3-*a*]quinoxalin-1-one Scaffold. *J. Med. Chem.* 2012; 55:1771–1782. [PubMed: 22277057]
31. Carosati E, Sforna G, Pippi M, Marverti G, Ligabue A, Guerrieri D, Piras S, Guaitoli G, Luciani R, Costi MR, Cruciani G. Ligand-based virtual screening and ADME-tox guided approach to identify triazolo-quinoxalines as folate cycle inhibitors. *Bioorg. Med. Chem.* 2010; 18:7773–7785. [PubMed: 20951595]
32. Ali I, Lee J, Go A, Choi G, Lee K. Discovery of novel [1,2,4]triazolo[4,3-*a*]quinoxaline aminophenyl derivatives as BET inhibitors for cancer treatment. *Bioorg. Med. Chem. Lett.* 2017; 27:4606–4613. [PubMed: 28939121]
33. Andres J-I, Buijnsters P, De Angelis M, Langlois X, Rombouts F, Trabanco AA, Vanhoof G. Discovery of a new series of [1,2,4]triazolo[4,3-*a*]quinoxalines as dual phosphodiesterase 2/ phosphodiesterase 10 (PDE2/PDE10) inhibitors. *Bioorg. Med. Chem. Lett.* 2013; 23:785–90. [PubMed: 23260348]
34. Lee S, Esteva-Font C, Phuan PW, Anderson MO, Verkman AS. Discovery, synthesis and structure-activity analysis of symmetrical 2,7-disubstituted fluorenones as urea transporter inhibitors. *MedChemComm.* 2015; 6:1278–1284. [PubMed: 26191399]

**Figure 1.**

(A) Structures and IC_{50} values of active UT-A1 inhibitors identified by high-throughput screening. (B) Strategy to explore structure–activity relationships of **8aa** analogues.

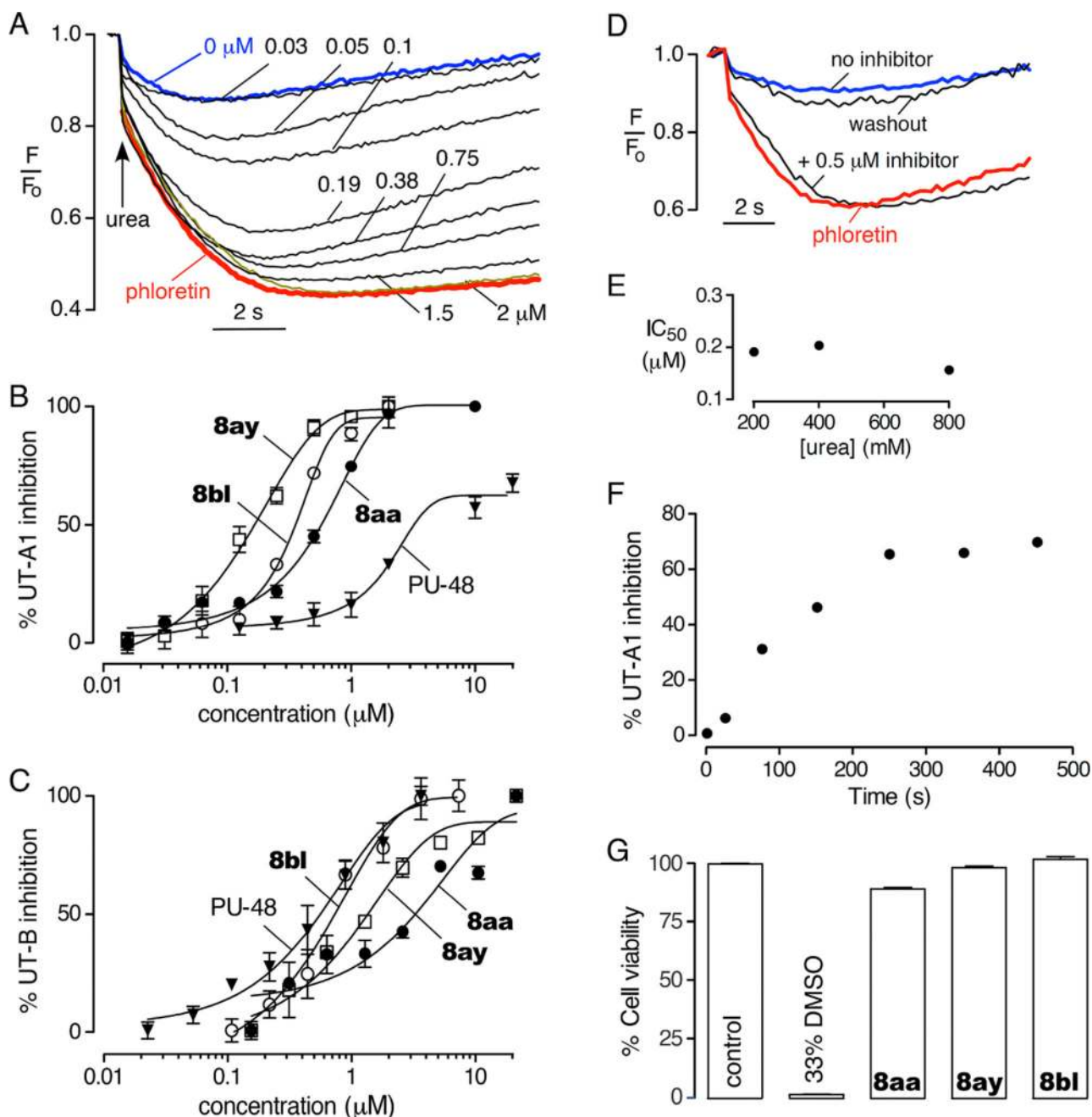


Figure 2.

In vitro characterization of UT-A inhibitors. (A) Original fluorescence data showing inhibition of rat UT-A1 by different concentrations of **8ay**. Positive (100% inhibition, phloretin, red curve) and negative (0% inhibition, DMSO vehicle, blue curve) curves are also shown. (B) Concentration–inhibition data for UT-A1 inhibition by the indicated compounds (mean \pm SEM, $n = 3$). (C) Concentration dependence data for UT-B inhibition by the indicated compounds (mean \pm SEM, $n = 3$). (D) Reversibility study. Cells were incubated with **8ay** at 0.5 μM for 15 min, washed for 15 min, and then assayed for UT-A1 inhibition. (E) Urea competition. Experiments were done as in (A) but with different urea

concentrations (200, 400, and 800 mM). (F) Kinetic study. Experiments were done as in (A) but at different times after addition of 0.5 μM **8ay**. (G) Cytotoxicity measured by AlamarBlue assay in transfected MDCK cells incubated for 24 h with 10 μM **8aa**, **8ay**, or **8bl** (mean \pm SEM, $n = 3$). The vehicle control result is also shown.

Author Manuscript

Author Manuscript

Author Manuscript

Author Manuscript

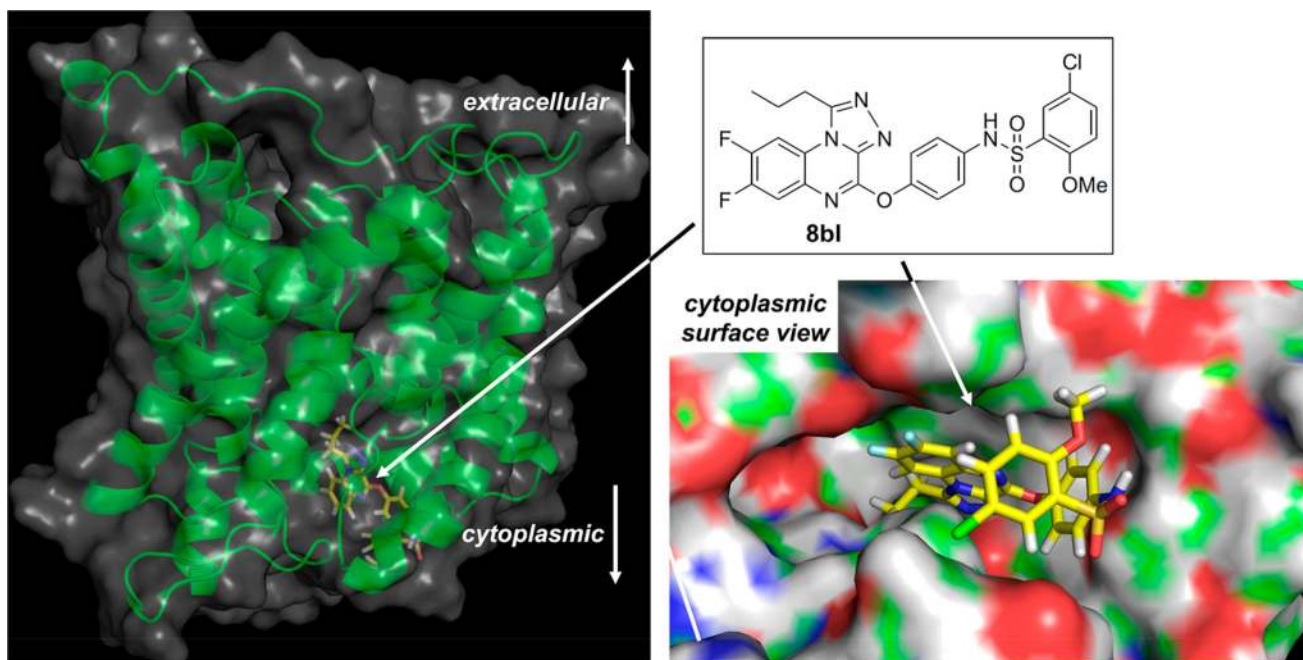


Figure 3. Computational modeling of triazoloquinoxaline inhibitor **8bl** bound to a homology model of rat UT-A1. Zoomed-out (left) and zoomed-in (right) representations of **8bl** interacting with the UT-A1 cytoplasmic domain show the complementary fit of the overall scaffold and the projection of the hydrophobic propyl group into the channel.

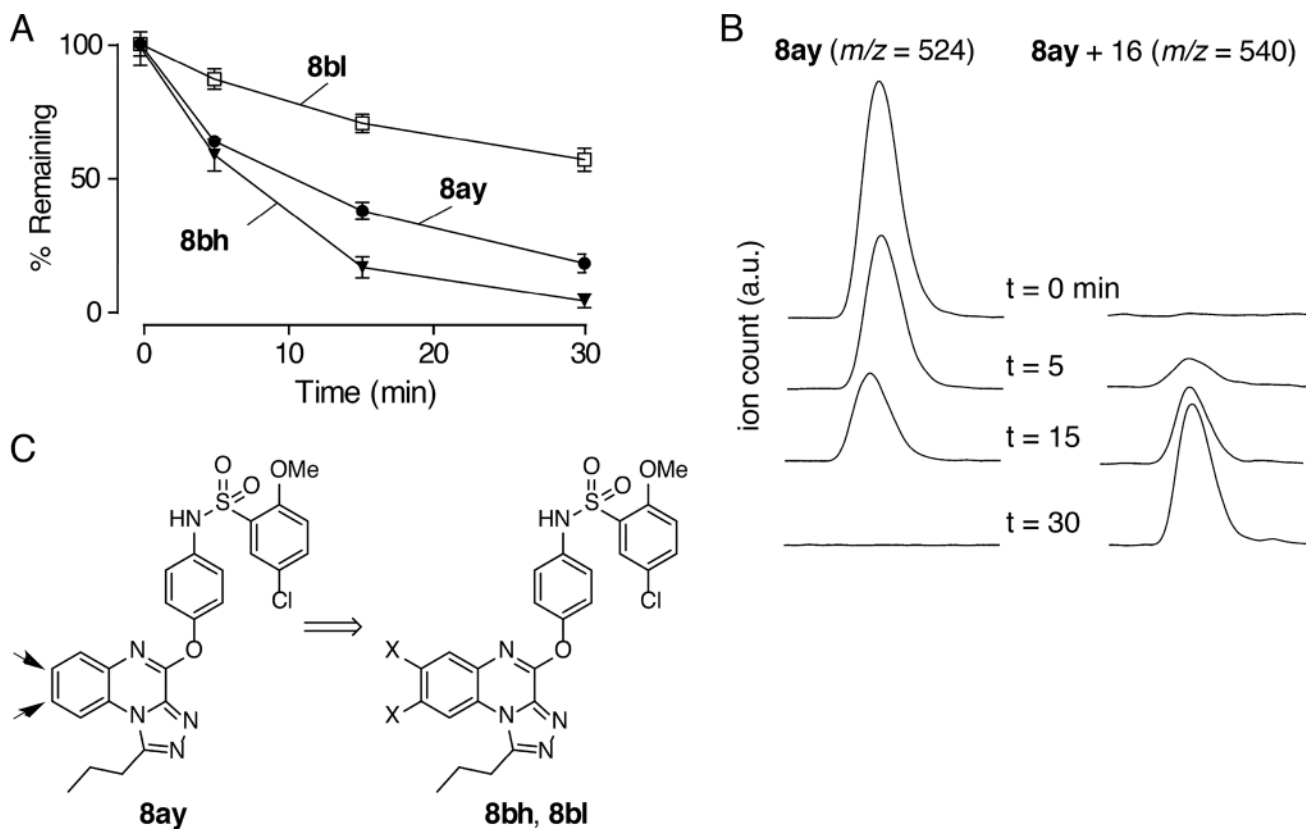


Figure 4.

In vitro metabolic stability in rat hepatic microsomes. (A) Compounds **8ay**, **8bh**, and **8bl** at 5 μM were incubated for the indicated times with 1 mg/mL rat hepatic microsomes in the presence of NADPH, and the parent compound was assayed by LC/MS (mean \pm SEM, $n = 3$). (B) LC/MS profile showing the disappearance of **8ay** over 30 min of incubation (left) and the appearance of metabolite at +16 Da (right). (C) Schematic of potential sites of metabolism.

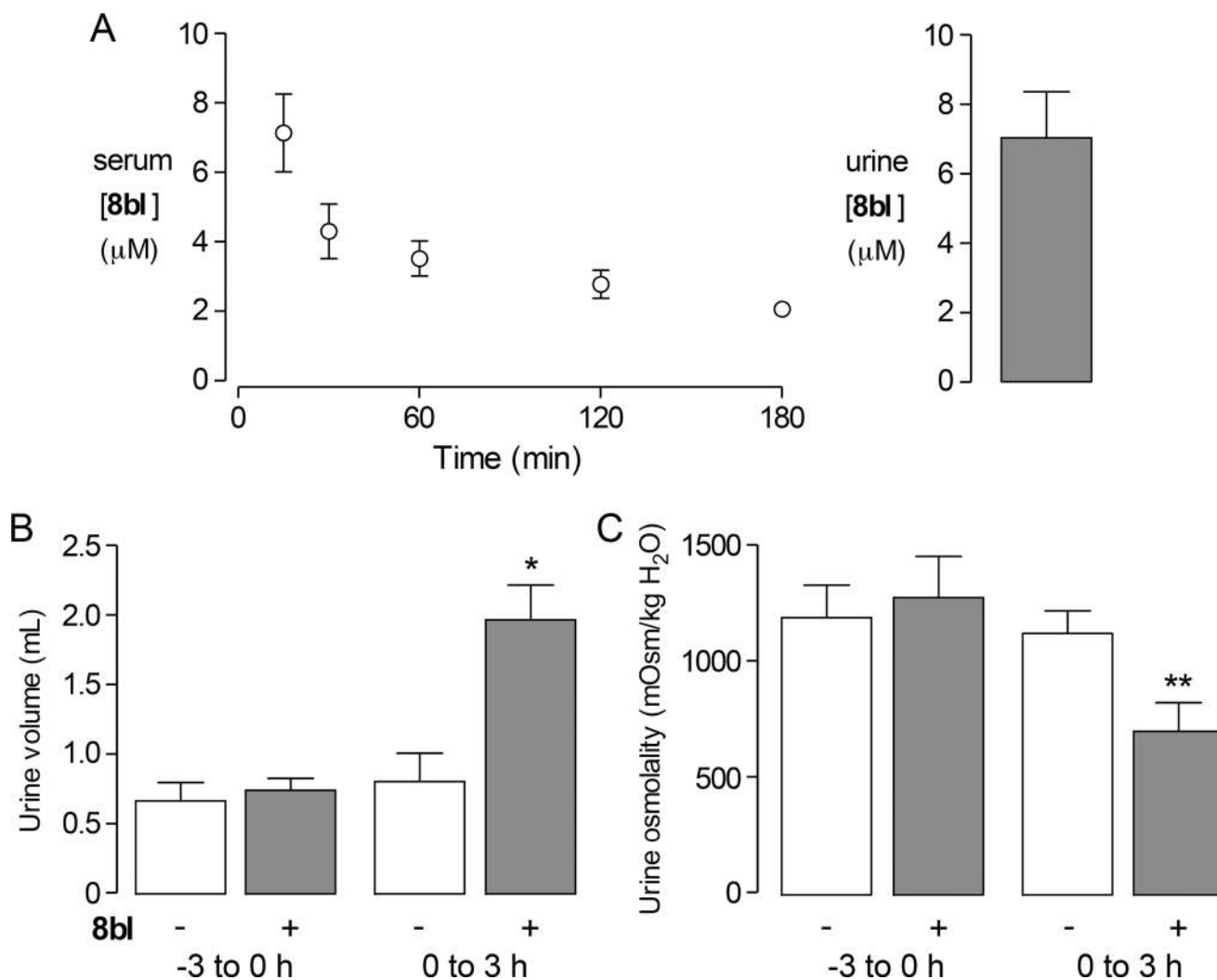
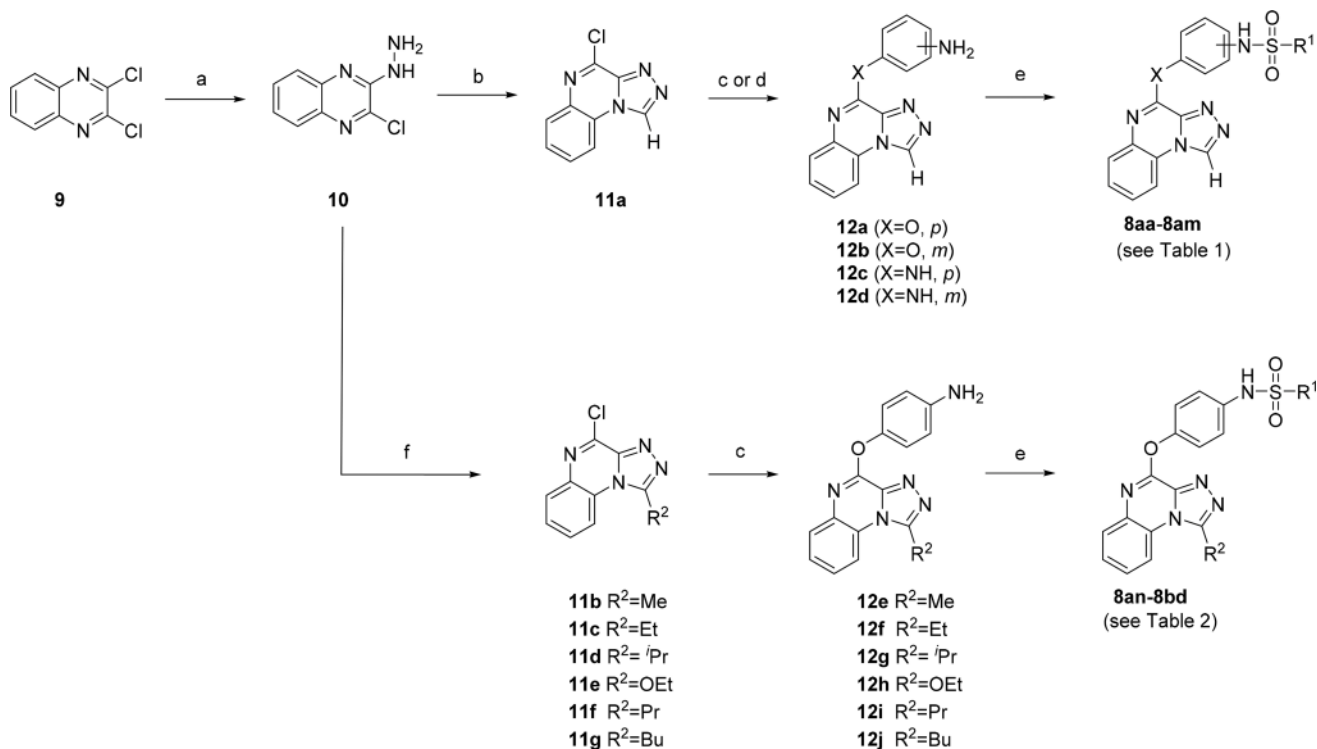


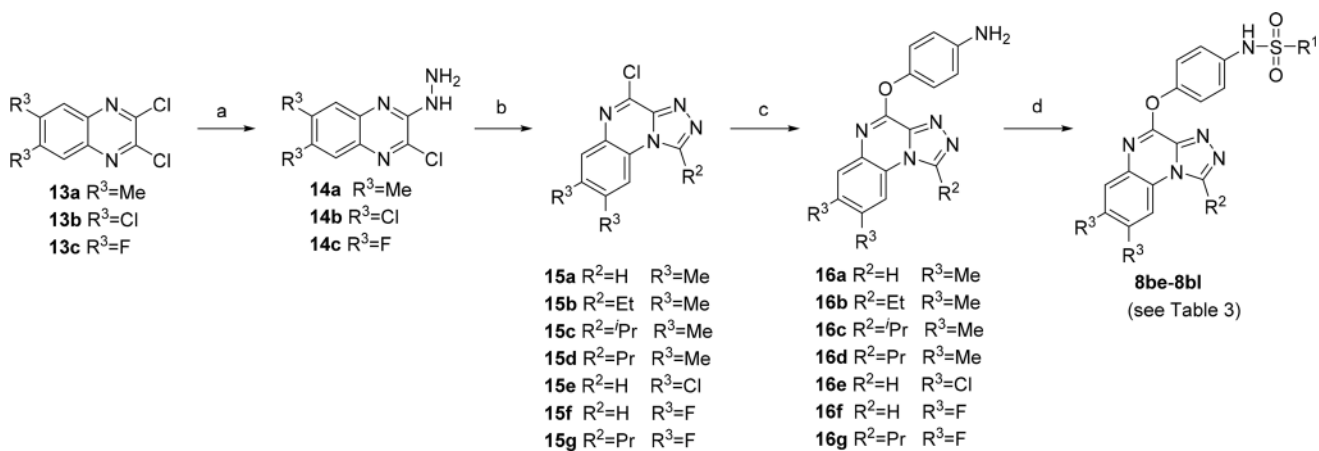
Figure 5.

In vivo pharmacokinetics of **8bl** and diuretic action in rats. (A) Kinetics of serum **8bl** concentration following intravenous administration of 4 mg/kg **8bl** (left) and **8bl** concentration in urine collected for 3 h (right). (B, C) 3 h urine volume (B) and osmolality (C) before and after intravenous administration of **8bl** or vehicle (mean ± SEM, $n = 4$). * $P < 0.01$ and ** $P < 0.05$ compared with -3 to 0 h (paired t-test).



Scheme 1. General Synthesis of 1,2,4-Triazoloquinoxalines^a

^aReagents and conditions: (a) NH₂NH₂, EtOH; (b) HC(OEt)₃, 100 °C; (c) *p*-aminophenol, Cs₂CO₃, DMSO, 50 °C; (d) *p*-phenylenediamine, K₂CO₃, DMSO; (e) R¹SO₂Cl, DIPEA, acetonitrile, 50 °C; (f) R²C(OMe)₃ or R²C(OEt)₃.

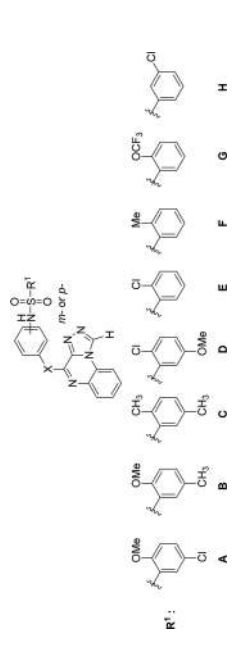


Scheme 2. Synthesis of 7,8-Disubstituted 1,2,4-Triazoloquinoxalines^a

^aReagents and conditions: (a) NH₂NH₂, EtOH; (b) R²C(OEt)₃ or R²C(OMe)₃, 100 °C; (c) *p*-aminophenol, Cs₂CO₃, DMSO, 50 °C; (d) R¹SO₂Cl, DIPEA, acetonitrile, 50 °C.

UT-A1 Inhibition by 1,2,4-Triazoloquinoxalines with Modifications in Parts A and B

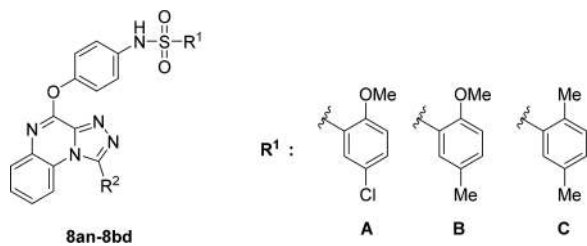
Table 1



compound	X	m- or p-	R ¹	isolated yield (%)	UT-A1 IC ₅₀ (μM)
8aa	O	<i>p</i> -	A	58	0.8
8ab	O	<i>m</i> -	A	35	>20
8ac	NH	<i>p</i> -	A	36	>20
8ad	NH	<i>m</i> -	D	91	>20
8ae	O	<i>p</i> -	B	99	1.1
8af	O	<i>p</i> -	C	82	1.5
8ag	O	<i>p</i> -	D	70	>20
8ah	O	<i>p</i> -	E	41	5
8ai	O	<i>p</i> -	F	97	8
8aj	O	<i>p</i> -	G	53	20
8ak	O	<i>p</i> -	H	87	>20
8al	O	<i>m</i> -	D	44	>20
8am	NH	<i>p</i> -	D	48	>20

Table 2

UT-A1 Inhibition by 1,2,4-Triazoloquinoxalines with Modifications in Part C



compound	R ¹	R ²	isolated yield (%)	UT-A1 IC ₅₀ (μM)
8an	A	CH ₃	47	>20
8ao	B	CH ₃	36	>20
8ap	C	CH ₃	48	>20
8aq	A	CH ₂ CH ₃	72	0.5
8ar	B	CH ₂ CH ₃	75	0.7
8as	C	CH ₂ CH ₃	77	0.75
8at	A	CH(CH ₃) ₂	48	0.3
8au	B	CH(CH ₃) ₂	60	0.5
8av	C	CH(CH ₃) ₂	87	0.6
8aw	A	OCH ₂ CH ₃	91	1.2
8ax	B	OCH ₂ CH ₃	63	1.5
8ay	A	CH ₂ CH ₂ CH ₃	39	0.15
8az	B	CH ₂ CH ₂ CH ₃	51	0.4
8ba	C	CH ₂ CH ₂ CH ₃	42	0.5
8bb	A	(CH ₂) ₃ CH ₃	37	0.2
8bc	B	(CH ₂) ₃ CH ₃	46	0.4
8bd	C	(CH ₂) ₃ CH ₃	49	0.8

Table 3

UT-A1 Inhibition by 1,2,4-Triazoloquinoxalines with Different R³

R¹ :

8be-8bl

compound	R ¹	R ²	R ³	isolated yield (%)	UT-A1 IC ₅₀ (μM)
8be	A	H	CH ₃	65	2.7
8bf	A	CH ₂ CH ₃	CH ₃	73	1.4
8bg	A	CH(CH ₃) ₂	CH ₃	99	1.2
8bh	A	CH ₂ CH ₂ CH ₃	CH ₃	80	0.4
8bi	A	H	Cl	70	>20
8bj	A	H	F	67	1.2
8bk	B	H	F	40	1.5
8bl	A	CH ₂ CH ₂ CH ₃	F	48	0.3